

Quantification of beam complexity in intensity-modulated radiation therapy treatment plans

Weiliang Du, Sang Hyun Cho, Xiaodong Zhang, Karen E. Hoffman, and Rajat J. Kudchadker

Citation: *Medical Physics* **41**, 021716 (2014); doi: 10.1118/1.4861821

View online: <http://dx.doi.org/10.1118/1.4861821>

View Table of Contents: <http://scitation.aip.org/content/aapm/journal/medphys/41/2?ver=pdfcov>

Published by the [American Association of Physicists in Medicine](#)

Articles you may be interested in

[Assessing software upgrades, plan properties and patient geometry using intensity modulated radiation therapy \(IMRT\) complexity metrics](#)

Med. Phys. **38**, 2027 (2011); 10.1118/1.3562897

[Treatment planning for volumetric modulated arc therapy](#)

Med. Phys. **36**, 5128 (2009); 10.1118/1.3240488

[Penalized likelihood fluence optimization with evolutionary components for intensity modulated radiation therapy treatment planning](#)

Med. Phys. **31**, 2335 (2004); 10.1118/1.1773631


[Clinical implementation of intensity-modulated tangential beam irradiation for breast cancer](#)

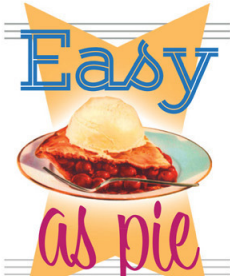
Med. Phys. **31**, 1023 (2004); 10.1118/1.1690195

[Beam orientation optimization in intensity-modulated radiation treatment planning](#)

Med. Phys. **27**, 1238 (2000); 10.1118/1.599001

RadImage.com - Helical Tomotherapy QA





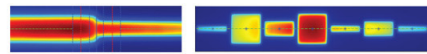
Easy
as pie

RITG148⁺

Custom Designed

TG-148 Tests


For Tomotherapy QA



RIT is your only source for the tests specified for helical tomotherapy in the TG-148 report. These automated QA tests include:

• Automated QA testing	• MLC alignment test
• Y-jaw divergence/beam centering	• Couch translation/gantry rotation
• Y-jaw/gantry rotation plane alignment	• Laser localization
• Gantry angle consistency	• Image quality tests (Cheese Phantom)
• Treatment field centering	• Built in trending and reporting with RITrend

These tests are included in both our RITComplete, and RITG148+ products.



radimage.com

Call 719.590.1077,
option 4, or email
mac@radimage.com
today to set up your
personal demo.

Quantification of beam complexity in intensity-modulated radiation therapy treatment plans

Weiliang Du,^{a)} Sang Hyun Cho, and Xiaodong Zhang

Department of Radiation Physics, The University of Texas MD Anderson Cancer Center, Houston, Texas 77030

Karen E. Hoffman

Department of Radiation Oncology, The University of Texas MD Anderson Cancer Center, Houston, Texas 77030

Rajat J. Kudchadker

Department of Radiation Physics, The University of Texas MD Anderson Cancer Center, Houston, Texas 77030

(Received 21 August 2013; revised 30 October 2013; accepted for publication 26 December 2013; published 21 January 2014)

Purpose: Excessive complexity in intensity-modulated radiation therapy (IMRT) plans increases the dose uncertainty, prolongs the treatment time, and increases the susceptibility to changes in patient or target geometry. To date, the tools for quantitative assessment of IMRT beam complexity are still lacking. In this study, the authors have sought to develop metrics to characterize different aspects of beam complexity and investigate the beam complexity for IMRT plans of different disease sites.

Methods: The authors evaluated the beam complexity scores for 65 step-and-shoot IMRT plans from three sites (prostate, head and neck, and spine) and 26 volumetric-modulated arc therapy (VMAT) plans for the prostate. On the basis of the beam apertures and monitor unit weights of all segments, the authors calculated the mean aperture area, extent of aperture shape irregularity, and degree of beam modulation for each beam. Then the beam complexity values were averaged to obtain the complexity metrics of the IMRT plans. The authors studied the correlation between the beam complexity metrics and the quality assurance (QA) results. Finally, the effects of treatment planning parameters on beam complexity were studied.

Results: The beam complexity scores were not uniform among the prostate IMRT beams from different gantry angles. The lateral beams had larger monitor units and smaller shape irregularity, while the anterior-posterior beams had larger modulation values. On average, the prostate IMRT plans had the smallest aperture irregularity, beam modulation, and normalized monitor units; the head and neck IMRT plans had large beam irregularity and beam modulation; and the spine stereotactic radiation therapy plans often had small beam apertures, which may have been associated with the relatively large discrepancies between planned and QA measured doses. There were weak correlations between the beam complexity scores and the measured dose errors. The prostate VMAT beams showed greater complexity than the prostate step-and-shoot IMRT beams. In the treatment planning process, the beam complexity increased as the minimum segment area decreased and as the number of optimization iterations and the maximum number of segments increased.

Conclusions: The proposed metrics were effective in characterizing the beam complexity of different disease sites and for different treatment modalities. Efforts should be made to reduce the unnecessary complexity of IMRT beams to minimize the radiation dose uncertainties. © 2014 American Association of Physicists in Medicine. [<http://dx.doi.org/10.1118/1.4861821>]

Key words: IMRT, VMAT, beam complexity, beam modulation

1. INTRODUCTION

Over the last two decades, the complexity of external beam radiation therapy has increased significantly. This is evidenced by the widespread use of intensity-modulated radiation therapy (IMRT) and, more recently, volumetric-modulated arc therapy (VMAT), a special form of IMRT. IMRT enables greater dose conformity to target tissues and spares more normal tissue than traditional three-dimensional conformal radiation therapy (3D-CRT); however, IMRT often leads to increased beam modulation, larger total monitor units (MU), longer treatment time, larger dosimetric uncertainty, and

increased susceptibility to setup errors and internal organ motion.¹⁻⁵

The complexity of IMRT plans arises from beam modulation. Most IMRT plans require a large number of small and/or irregularly shaped beam segments to achieve high dose conformity. These small beam segments carry higher dose uncertainties than those found in the large fields used in 3D-CRT. The output factors and the penumbra of small beams are challenging to measure accurately.⁶⁻¹¹ In addition, the use of multileaf collimator (MLC)-shaped beam segments in IMRT requires accurate modeling of leaf end, leaf transmission, and interleaf leakage.^{1,2} In 2008, the Radiological Physics

Center reported that approximately 28% of institutions applying for IMRT credentialing failed to deliver a planned dose distribution to a head and neck (HN) phantom, using the 7% and 4 mm dose-distance agreement criteria.¹² Among various sources of potential errors, the complexity of IMRT plans is related to delivery accuracy, with increased complexity leading to a decreased passing rate in IMRT quality assurance (QA).^{13–15}

Evaluation and reduction of IMRT plan complexity have been an interesting research area. A commonly used indicator of plan complexity is the total plan MU (i.e., the sum of the MUs from all beams). For example, a typical IMRT plan for prostate cancer treatment has a total MU of 660, while a 3D-CRT plan for the same patient may have a total MU of 220. The threefold difference in total MU is a clear indication of the complexity in the IMRT plan. Although the total MU is a quick measure of beam modulation, it does not provide any distinction among the different forms of plan complexity: small beam segments, irregularly shaped and narrow beam segments, or a large number of beam segments. In addition, the total MU does not reflect the complexity of individual IMRT beams.

Other plan complexity metrics fall into two categories: fluence map-based and aperture-based. The best known fluence map-based metric is the modulation index (MI) proposed by Webb.¹⁶ MI measures the variations of photon fluence between neighboring pixels in the fluence map of a given beam. Nauta *et al.*¹³ proposed that fluence maps can be assessed with fractal analysis. Coselmon *et al.*¹⁷ quantified beam modulation using a metric called plan intensity map variation. A limitation of fluence map-based approaches is their insensitivity to the degeneracy of fluence maps. For example, a large beam can be decomposed spatially into many small beam segments so that the large beam and the sum of small beam segments generate the same fluence map. The resulting MI would be identical in these two situations, even though the IMRT beam composed of many small beam segments is apparently more complex than the single large beam. Aperture-based approaches assess beam complexity by directly analyzing the beam apertures. McNiven *et al.*¹⁸ proposed a modulation complexity score (MCS), which consisted of leaf sequence variability (LSV) and aperture area variability (AAV). These parameters were calculated from the MLC leaf positions and segment weights. McGarry *et al.*¹⁹ compared various published complexity metrics and found that MCS was more sensitive than MU, plan intensity map variation, and MI in terms of detecting the changes in beam complexity between treatment planning system (TPS) upgrades or between plans created for different planning parameters and treatment sites. Younge *et al.*¹⁵ utilized edge metric, an aperture-based metric, to penalize beam complexity in VMAT inverse planning. The aperture-based metrics^{15,18} are mostly composite, i.e., assigning a single complexity score for one IMRT beam or the entire plan. The metrics usually combine different beam parameters such as leaf gap, edge length, and aperture area into one complexity score.

A simple IMRT beam consists of a few large beam apertures of regular shapes. Conversely, a complex IMRT beam

may have small beam apertures, narrow or irregular apertures, excessive number of apertures, or any combination of the above. Despite the previously reported beam complexity metrics, few tools other than the total MU are widely available for medical physicists to quantify and reduce the complexity in IMRT plans. It is the authors' opinion that a single composite metric cannot reveal the details of the complexity in IMRT plans or beams. We aimed to address this problem by developing multiple metrics to quantify different aspects of beam complexity, including aperture area, aperture shape irregularity, and beam modulation. Using these quantities, we compared beam complexity for different treatment sites and modalities, including prostate IMRT, HN IMRT, spine IMRT, and prostate VMAT. We also investigated the effects of planning parameters on beam complexity and correlated beam complexity with IMRT QA measurements.

2. MATERIALS AND METHODS

2.A. Beam complexity metrics

The method developed in this study is aperture-based, which means that all metrics are calculated from the IMRT plan information including leaf positions, MU of individual beam segments, jaw sizes, and prescribed dose. We extracted the IMRT plans from the treatment record and verification system MOSAIQ (IMPAC Medical Systems, Sunnyvale, CA). For each patient, the IMRT plan was exported and saved into a text file in the RTP format. Then the text file was processed in MATLAB (MathWorks, Natick, MA) to generate complexity metrics below.

For the j th aperture (herein interchangeable with “segment”) A_{ij} in a given beam i , the aperture area (AA) is computed as the total area of all MLC openings within A_{ij} [Fig. 1(a)].

$$AA_{ij} = \sum_{k=1}^{N_{LP}} t_k \cdot (x_{2ijk} - x_{1ijk}), \quad (1)$$

where k is the index number of leaf pairs, N_{LP} is the total number of leaf pairs, t_k is the width of the k th leaf pair, x_{1ijk} and x_{2ijk} are the positions of the k th leaf pair relative to the beam isocenter. Any MLC openings outside the rectangular field defined by the jaws are discarded.

The aperture perimeter (AP) is computed in a similar manner [Fig. 1(a)]. The aperture irregularity (AI) is obtained by calculating the noncircularity of the aperture:

$$AI_{ij} = \frac{AP_{ij}^2}{4\pi \cdot AA_{ij}}. \quad (2)$$

AI is 1 if the aperture is a perfect circle or greater than 1 otherwise. For a square field, AI is $4/\pi$, or 1.273. For a narrow aperture that is often used in sliding-window IMRT, AI is an indicator of aperture narrowness (i.e., the greater the AI value, the narrower the aperture).

After the AA, AP, and AI for each segment in beam i are obtained, the beam complexity metrics can be computed. For example, the beam area (BA) is computed as

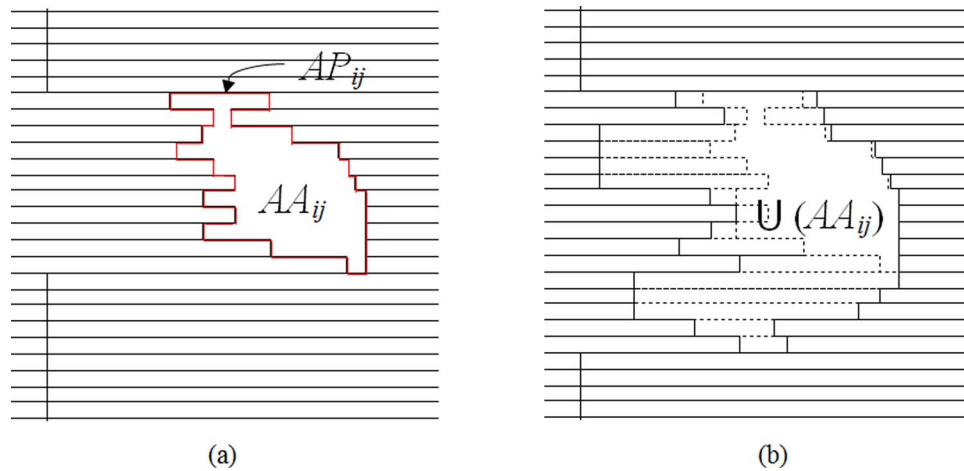


FIG. 1. Schematic illustration of the beam aperture analysis. (a) The j th segment A_{ij} of beam i . AA_{ij} and AP_{ij} in Eqs. (1) and (2) are the area and perimeter (red boundary) of A_{ij} , respectively. (b) $U(AA_{ij})$ is the union area of all segments in beam i . The MLC leaves that form A_{ij} are shown in dashed lines for comparison.

$$BA_i = \frac{\sum_j (MU_{ij} \cdot AA_{ij})}{MU_i}, \quad (3)$$

where MU_{ij} and MU_i are the MU of segment A_{ij} and beam i , respectively. Similar to Eq. (3), the beam irregularity (BI) is computed using AI_{ij} , MU_{ij} , and MU_i . Beam modulation (BM) is computed as

$$BM_i = 1 - \frac{\sum_j (MU_{ij} \cdot AA_{ij})}{MU_i \cdot U(AA_{ij})}. \quad (4)$$

$U(AA_{ij})$ is the union area of all apertures of beam i [Fig. 1(b)]. By definition, the union area of all apertures is greater than or equal to the area of any individual aperture. Thus, BM ranges from 0 to 1. For a simple 3D-CRT beam without modulation, $BM = 0$. For a beam consisting of many small apertures that are spatially separated from each other, BM approaches 1.

The plan averaged beam complexity metrics are synthesized from the individual beam metrics. For example, the plan averaged beam area (PA) is computed as

$$PA = \frac{\sum_i (BA_i \cdot MU_i)}{MU_p}, \quad (5)$$

where MU_p is the total MU in the plan. Similarly, the plan averaged beam irregularity (PI) and the plan averaged beam modulation (PM) are obtained by averaging the BI values or BM values using the beam MUs as weighting factors.

To compare the total MU among IMRT plans with different prescription dose levels, we normalize the total MU by the fractional target dose, yielding the plan normalized MU (PMU):

$$PMU = \frac{MU_p \cdot 2 \text{ Gy}}{d}, \quad (6)$$

where d is the prescribed target dose per fraction, in Gy. For all prostate and HN IMRT plans in this study, $d = 2.0 \pm 0.2$ Gy. For the spine stereotactic plans, $d = 9$ Gy for the three-fraction regimen and 18 or 24 Gy for the one-fraction regimen.

2.B. Treatment plans

To test the utility of the presented complexity metrics, we retrospectively selected 65 IMRT plans from three treatment sites: prostate ($N = 22$), HN ($N = 20$), and spine ($N = 23$). All these plans were created by medical dosimetrists in the Pinnacle³ TPS (Philips, Fitchburg, WI) using the step-and-shoot IMRT modality. The targets in the prostate plans were the prostate and the proximal seminal vesicle, or the involved fossa if the prostate had been surgically removed. Patients with pelvic nodal treatments were excluded from this study. Our standardized gantry angles used in prostate IMRT plans were 225°, 260°, 295°, 330°, 30°, 65°, 100°, 135°, and 180 degrees. The targets of the HN plans included a variety of sites such as the base of the tongue, larynx, nasopharynx, mandible, and tonsil. The patients receiving spinal irradiation underwent stereotactic body radiation therapy using one- or three-fraction regimens, and the targets were metastatic tumors involving one ($N = 14$) or more ($N = 5$) spinal vertebrae or the sacrum ($N = 4$). The spine plans were characterized by a high dose to a relatively small target and a fast dose fall-off from the target to the critical structure: either the spinal cord or the cauda equina.

To compare step-and-shoot IMRT and VMAT, we selected additional prostate patients treated with VMAT ($N = 26$). Two arcs, each with 300° gantry rotation, were used in the prostate VMAT plans.

For each plan, the following quantities were computed: AA, AP, and AI for each segment; BA, BI, and BM for each beam; and PA, PI, PM, and PMU for each plan. Then we performed two-sided Wilcoxon rank sum tests on the PA, PI, PM, and PMU data. The p-values were computed in MATLAB and p-values of 0.05 or less were considered statistically significant.

To correlate the complexity metrics and the dose delivery accuracy, the IMRT QA results were retrospectively collected for all step-and-shoot IMRT patients. The pre-treatment IMRT QA was performed on a body phantom (IBA Dosimetry, Schwarzenbruck, Germany). A Wellhofer CC-04 (0.04 cc) ion chamber was inserted to the center of the phantom.

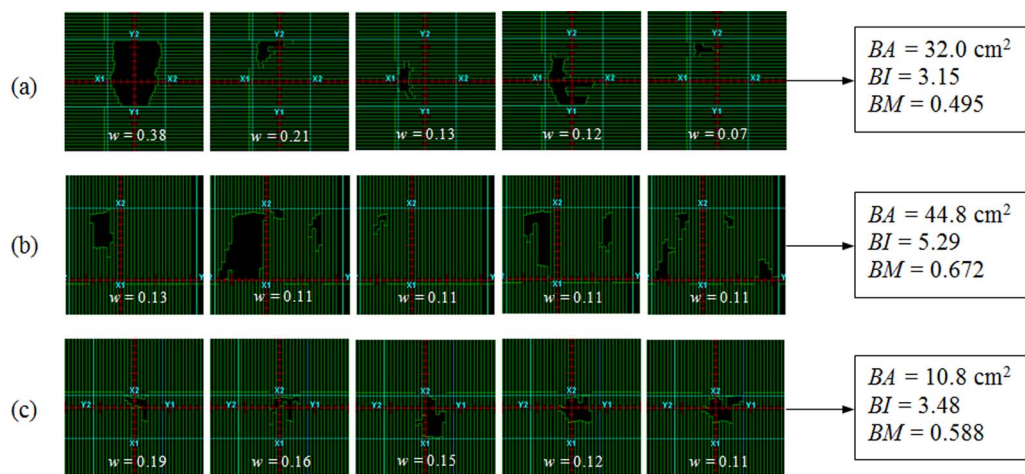


FIG. 2. Segments of typical prostate (a), HN (b), and spine (c) beams. Only five segments of the largest MU weights (w) are displayed for each beam. BA, BI, and BM were quantified on the basis of the apertures and the MU weights.

The dose distribution in an axial plane was also measured on a piece of radiographic film. The planned isocenter was set so that the ion chamber was located in a high dose region with small dose gradients. The difference between the ion chamber measured dose and the TPS-calculated dose was determined as a percentage of the planned dose. A discrepancy within $\pm 3\%$ was considered acceptable. The film passing criterion was $\geq 90\%$ of analyzed pixels had gamma (3 mm, 5%) ≤ 1 . The ion chamber measured dose errors and the film passing rates were correlated with PA, PI, PM, and PMU by calculating the corresponding Spearman's rank correlation coefficients.

To study the impact of planning parameters on beam complexity, we randomly selected one prostate IMRT plan and made modifications. For each modification, we changed only one planning parameter and computed the complexity metrics from the resulting IMRT plan. The planning parameters included in this study were the number of optimization iterations, the minimum segment area, and the maximum number of segments.

3. RESULTS

Table I shows the beam complexity results obtained from the prostate IMRT plans. The data suggested that the beam

TABLE I. Beam complexity scores (mean \pm standard deviation) of prostate IMRT plans. BA = beam area, BI = beam irregularity, and BM = beam modulation.

Gantry angle (deg)	MU	BA (cm ²)	BI	BM
225	52 \pm 15	29.7 \pm 6.7	3.85 \pm 0.74	0.43 \pm 0.10
260	103 \pm 21	28.3 \pm 7.3	3.33 \pm 0.42	0.45 \pm 0.11
295	68 \pm 22	32.0 \pm 6.4	3.68 \pm 0.66	0.39 \pm 0.09
330	67 \pm 23	28.4 \pm 9.2	3.73 \pm 0.58	0.55 \pm 0.12
30	70 \pm 23	27.5 \pm 9.9	3.85 \pm 0.58	0.57 \pm 0.11
65	66 \pm 19	31.0 \pm 7.1	3.61 \pm 0.49	0.40 \pm 0.12
100	102 \pm 20	26.6 \pm 7.9	3.27 \pm 0.49	0.49 \pm 0.11
135	51 \pm 13	31.8 \pm 8.0	3.77 \pm 0.77	0.40 \pm 0.13
180	68 \pm 22	28.7 \pm 10.7	4.11 \pm 0.63	0.61 \pm 0.13

complexity was not uniform across different beam angles. The two beams with the largest MUs were from gantry angles 260° and 100°. The same two beams had the least irregularity in aperture shapes. There were no significant differences in beam areas among different gantry angles. Beam modulation was the highest with gantry angles 180°, 330°, and 30°. The varied beam complexities are probably due to the special planning geometry in prostate IMRT, that is, the primary normal structures (rectum and bladder) are anterior or posterior to the target.

Figure 2 shows the segments of typical prostate, HN, and spine IMRT beams. The prostate beams usually had one or a few dominant segments with large areas and high MU weights. The HN beams generally had large union areas; however, each segment was more likely to consist of isolated areas that were much smaller than the union areas. The spine beams were generally characterized by the small apertures.

In Fig. 3 the plan averaged beam complexity metrics from the 65 step-and-shoot IMRT plans are plotted. Figure 3(a) shows that, on average, the spine plans had the smaller PA values than the prostate and HN plans. PI was generally higher in the HN plans than in the prostate plans; PI values were diverse in the spine plans. In Fig. 3(b), the PM was the lowest in the prostate plans and the highest in the HN plans. The PMU differences among treatment sites were not obvious. However, the spine plans showed a large variation in PMU, and the only three plans with greater than 1000 PMU were all spine plans.

Figure 4 compares the plan averaged beam complexity of step-and-shoot IMRT and VMAT for the prostate patients evaluated in this study. It is clear that the PI and PM were higher in the VMAT plans than in the IMRT plans. For comparison, Fig. 4(b) also shows a hypothetical data point of a four-field-box 3D-CRT plan, which had no beam modulation (i.e., PM = 0) and a PMU of approximately 220.

Table II summarizes the beam complexity metrics from the four groups of treatment plans. To illustrate the differences among the three treatment sites and the two treatment modalities, the p-value results from the statistical comparisons of

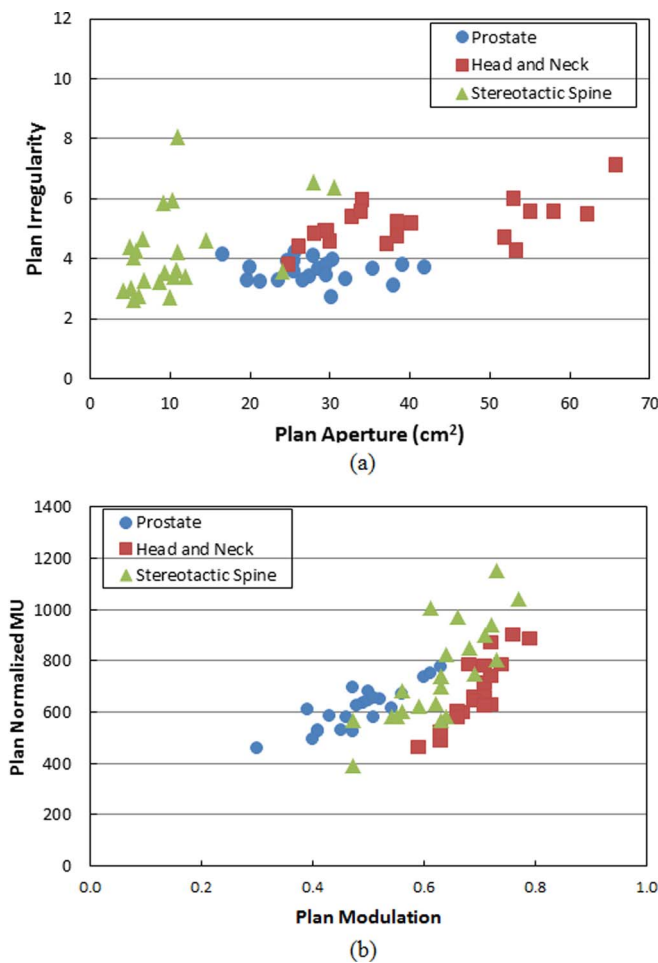


FIG. 3. Scatter plots of beam complexity metrics for three sites of IMRT treatments: prostate (circles), HN (squares), and spine (triangles). Plots show PA vs PI (a) and PM vs PMU (b).

the complexity metrics are provided in Table III. In agreement with Figs. 3 and 4, Tables II and III show that the spine plans had the smallest PA; the HN plans had the largest PM and PI; and the prostate VMAT plans had larger PM and PI than the prostate IMRT plans.

Figure 5 shows the plots of absolute dose discrepancy between the ion chamber measurements and the TPS calculations. The correlation coefficients (and p-values) were -0.38 (0.0009), -0.004 (0.51), 0.21 (0.05), 0.22 (0.04) between the absolute dose errors and PA, PI, PM, PMU, respectively. For the prostate IMRT plans, the dose discrepancy tended to increase with decreasing PA and increasing PI, PM, and PMU. The only two plans with $>3\%$ dose discrepancy were from spine IMRT plans. All film measurements passed

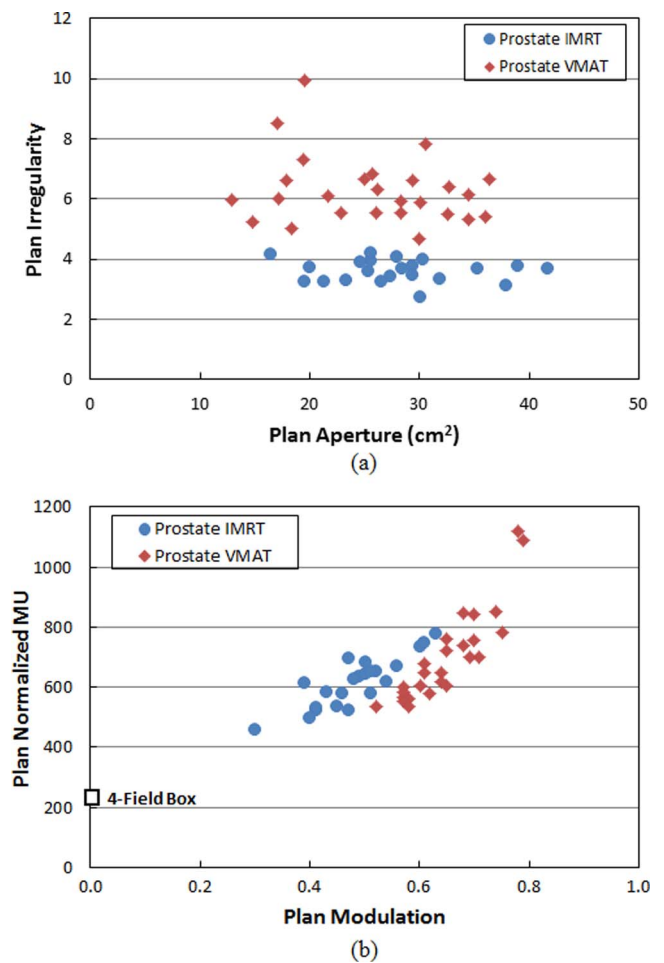


FIG. 4. Scatter plots of beam complexity metrics for two modalities of prostate treatments: step-and-shoot IMRT (circles) and VMAT (diamonds). Plots show PA vs PI (a) and PM vs PMU (b).

the criterion that $\geq 90\%$ of analyzed pixels had gamma ≤ 1 ; however, the percent passing rates had no correlation with the calculated complexity metrics (see Sec. 4).

Figure 6 shows that the beam complexity could be affected by adjusting the planning parameters. When the planner used a smaller minimum segment area, the IMRT optimization resulted in decreased PA and increased PM and PMU. Using a larger number of iterations for IMRT optimization decreased the PA and increased the PMU. The beam complexity increased slowly with increased number of iterations. When the maximum number of segments was increased, the plan complexity increased, as indicated by decreased PA and increased PI, PM, and PMU. After a certain number of segments [~ 70 in Fig. 6(c)] were reached, the beam complexity metrics became

TABLE II. Plan averaged beam complexity scores (mean \pm standard deviation) for the four groups of IMRT or VMAT plans.

Group	No. of plans	PA	PI	PM	PMU
Prostate IMRT	22	28.0 ± 6.4	3.61 ± 0.37	0.484 ± 0.078	617 ± 84
HN IMRT	20	41.1 ± 13.0	5.13 ± 0.74	0.695 ± 0.047	681 ± 127
Spine IMRT	23	10.7 ± 7.2	4.22 ± 1.44	0.629 ± 0.079	753 ± 188
Prostate VMAT	26	25.7 ± 6.95	6.29 ± 1.15	0.648 ± 0.071	702 ± 154

TABLE III. P-values obtained in comparing the beam complexity metrics for different disease sites (prostate versus HN versus spine) and treatment modalities (prostate step-and-shoot IMRT versus prostate VMAT). Bold font indicates p-values of statistical significance.

	PA	PI	PM	PMU
IMRT: prostate vs HN	5.3×10^{-4}	8.7×10^{-8}	5.5×10^{-8}	1.3×10^{-1}
IMRT: prostate vs spine	6.2×10^{-7}	4.0×10^{-1}	3.7×10^{-6}	1.0×10^{-2}
IMRT: HN vs spine	6.9×10^{-8}	3.3×10^{-3}	5.1×10^{-3}	2.7×10^{-1}
Prostate: IMRT vs VMAT	3.8×10^{-1}	3.5×10^{-9}	1.2×10^{-7}	5.7×10^{-2}

plateaued. For reference, we used the minimum segment area of 4 cm², the iteration count of 40, and the maximum number of segments of 50 in the original IMRT plan.

4. DISCUSSION

In this study, the complexity of IMRT beams was quantified by several metrics: aperture area, aperture shape irregularity, and degree of beam modulation. These metrics have straightforward physical meanings and can be easily com-

puted. For example, BA can be roughly understood as the average area of beam apertures, BI describes the deviations of the aperture shapes from a circle, and BM reflects the extent of a large open field being broken into multiple small segments. These interpretations suggest that the beam complexity increases with decreased BA, increased BI, and increased BM.

In IMRT treatment planning, a highly conformal dose distribution is often desired. One approach to achieving high conformity is to use many small beams. The rationale is that

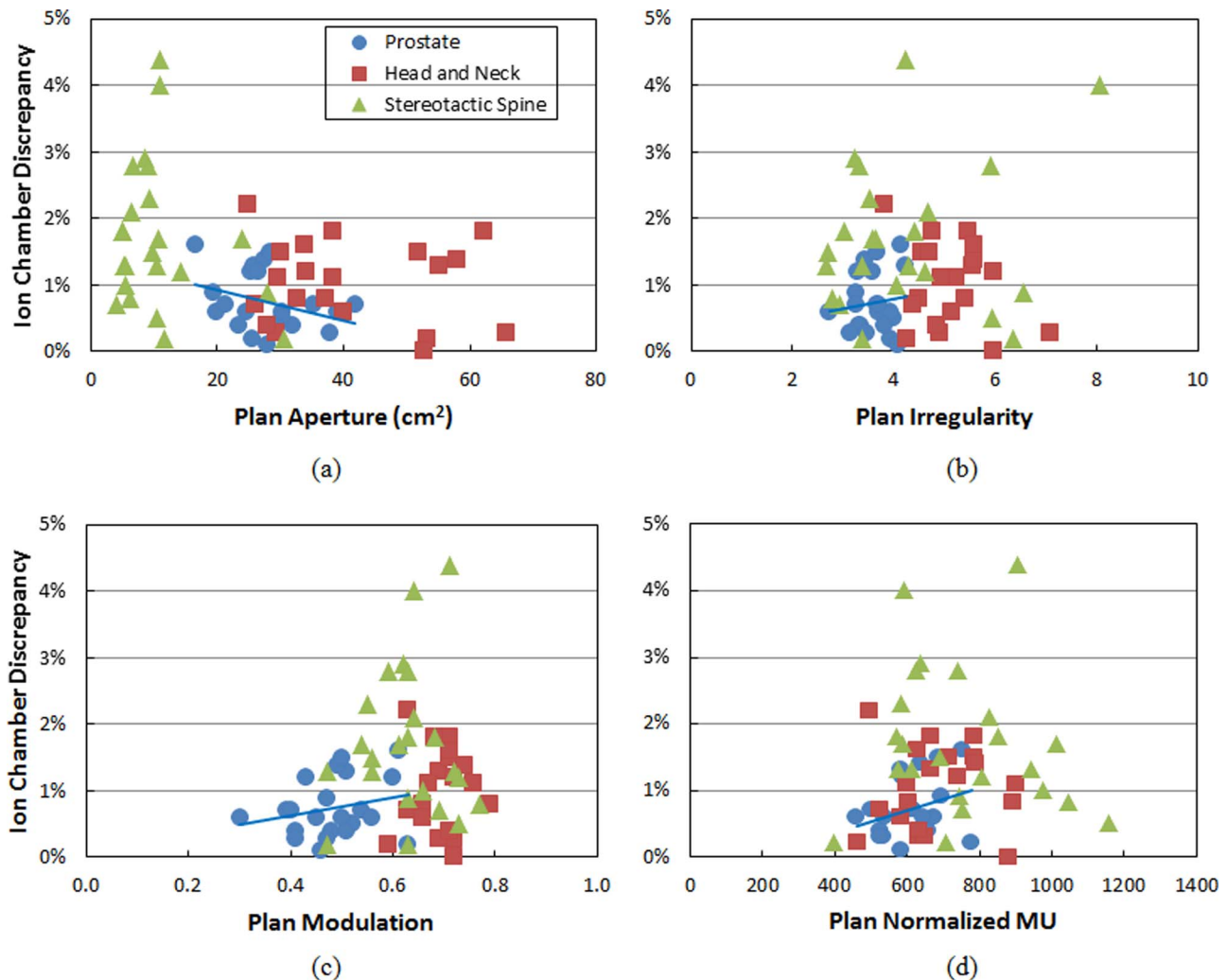


FIG. 5. Correlation of IMRT QA ion chamber results and complexity metrics: PA (a), PI (b), PM (c), and PMU (d). The linear trend lines are added to fit the prostate data points (circles) only.

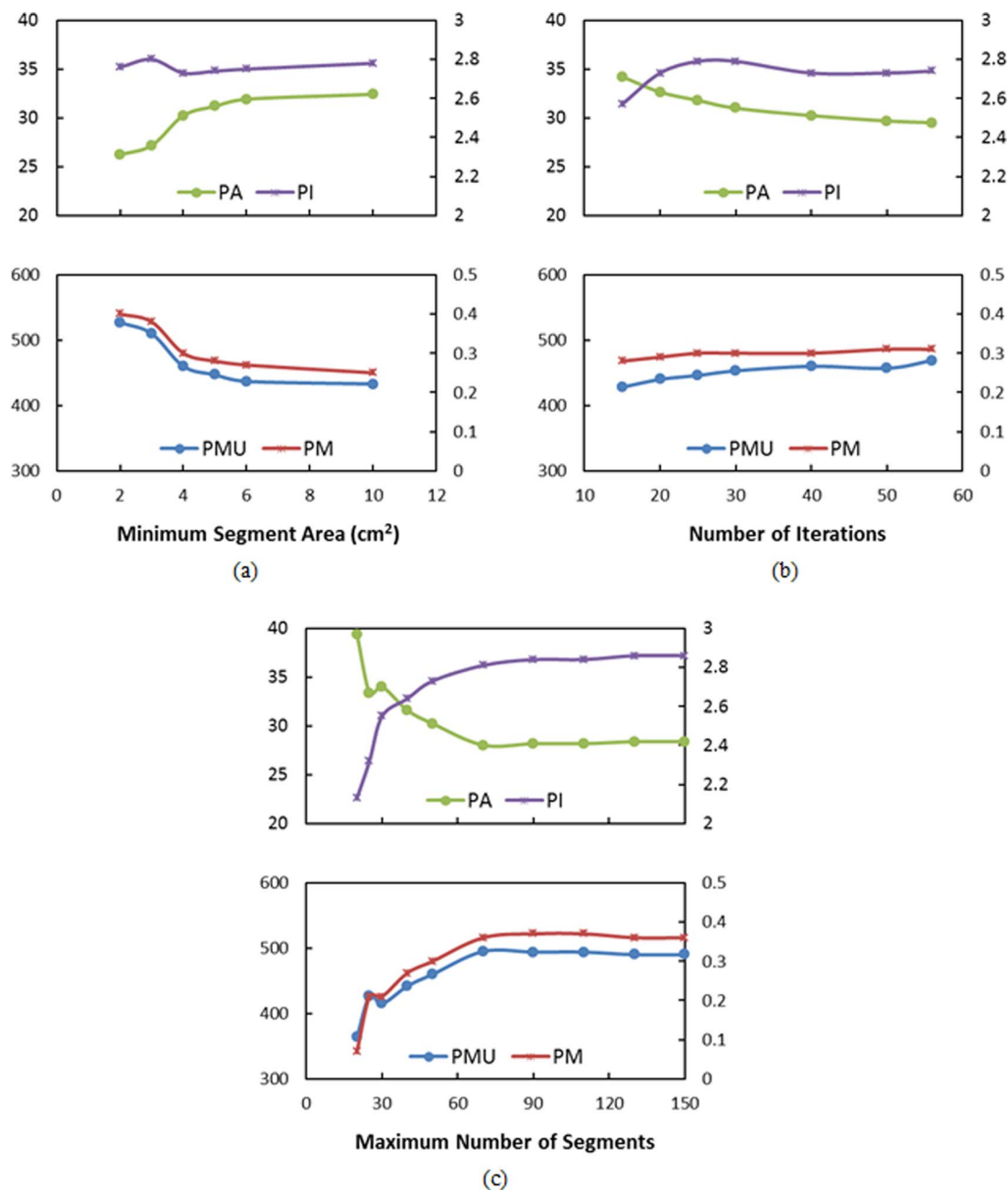


FIG. 6. Effects on PA, PI, PM, and PMU due to changes in minimum segment area (a), number of iterations during IMRT optimization (b), and maximum number of segments (c).

by dividing the beam into many small pieces, the number of degrees of freedom in IMRT optimization increases, thus making it easier to achieve high conformity. The drawbacks of this approach are numerous, including extended treatment time and increased susceptibilities to machine mechanical and dosimetric imperfections, patient setup errors, organ motion, etc. In this study we intended to discourage this many-small-beams approach by assigning high complexity scores to the IMRT plans generated with this approach. For these plans, BA would be small and BM would be large.

To the best of our knowledge, this paper is among the first to use the absolute beam area as a complexity indicator. Other metrics similar to beam area can be found in the previous

studies. For example, McNiven *et al.*¹⁸ investigated the effect of field size on IMRT QA passing rate. They used the number of diodes on the MapCheck array to represent the field size. This representation is limited in accuracy because of nonuniform spatial distribution of the diodes on the device. Nauta *et al.*¹³ employed the concept of average leaf gap when comparing four different complexity metrics. The leaf gap width and the beam area are related, but they are distinct quantities. The leaf gap width is one-dimensional in nature, whereas BA is two-dimensional. It is possible that a beam aperture has a large width and a small area by having a small length. Younge *et al.*¹⁵ showed a weak correlation between the aperture area and the percent of pixels with >10% measured dose errors.

They demonstrated that their proposed edge metric was more robust than the aperture area in predicting the dose errors.

The uncertainty of small beam dosimetry has gained increasing awareness over the recent years. Some institutions set a threshold for the minimum segment area in IMRT optimization. This practice is effective in limiting the use of small beam segments; however, the inverse planning algorithm may circumvent this limit by generating narrow, irregular apertures with an area satisfying the minimum segment area requirement. Like small apertures, narrow or irregular apertures can introduce dose uncertainties. We proposed the BI metric to quantitate the narrowness or irregularity of beam apertures. Conceptually, BI is similar to the edge metric proposed by Younge *et al.*¹⁵ or the LSV metric by McNiven *et al.*¹⁸ A quick dimensional analysis shows that the edge metric is not dimensionless. In other words, the edge metric depends not only on the shape of the aperture but also on the area. In contrast, BI depends on the shape of the aperture only. The rationale of our BI definition is to make BI independent of the metric BA, which is dedicated to characterize the beam area. Comparing to BI, LSV quantifies the variation of adjacent leaf positions, which is not necessarily the narrowness of beam apertures. For example, a narrow rectangular MLC field has LSV of 1, or zero complexity, whereas its BI value is larger than that for a simple square or circular field. Our BM metric is similar to the AAV metric by McNiven *et al.*¹⁸ A subtle computational difference exists in calculating the union area of all apertures of the beam. The denominator in Eq. (A3) of Ref. 18 seems to overestimate the union area if the leaf opening in one aperture does not overlap with the leaf openings from other apertures of the same beam.

IMRT beam complexity is often reported as a single index value, ranging from 0 to 1. This single-index approach is useful for quick comparison of one plan to another. However, it is not easy to distinguish the actual sources of the complexity with this approach. For example, the same high beam complexity scores may be the result of using narrow radiation fields, as in sliding-window IMRT treatments, or of using many small beam apertures, as in stereotactic spine radiation therapy. In our method, the two types of beam complexity are readily differentiated with a large BI in the former case and a small BA in the latter.

Quantification and control of IMRT beam complexity can be a difficult task. There are two inherent challenges in this process. First, each IMRT plan has a unique planning geometry, even when the disease site is the same. The plans in each subgroup of patients show significant variations in most complexity metrics (Figs. 3 and 4), which are likely due to variations in patient anatomy, dose constraints, and planning strategy. Nonetheless, there are some general observations in our data. On average, the prostate plans had the smallest PI, PM, and PMU; the HN plans had large PA, PI, and PM; the spine plans generally had small PA and large variations in PI, PM, and PMU. In addition, the spine plans were more likely to have large discrepancies between the planned and IMRT QA measured doses. These findings are useful for us to understand the beam characteristics of certain groups of IMRT plans. Second, the complexity is partly driven by factors in

inverse planning algorithms, which appear to be a “black box” to the treatment planner. Although beam complexity is expected to be minimized in “good” inverse planning algorithms, we found that the treatment planner can inadvertently cause increased beam complexity. Quantitative measures of beam complexity can be used as a tool to monitor and reduce the unreasonable complexity in IMRT plans.

It is interesting to compare the complexity of VMAT and IMRT beams for the same disease site. VMAT uses many more gantry angles than the traditional static gantry IMRT. At certain gantry angles, the beam may not be able to reach the target without passing through critical normal tissues. Thus, the MLC apertures at these gantry angles are narrowly opened or even closed. In the meantime, the union aperture area of the VMAT beam is larger than that of each IMRT beam because the VMAT beam approaches the target from many angles. These VMAT conditions result in increased PI, PM, and PMU, as indicated in Fig. 4 and Table II. Nonetheless, we do not indicate that VMAT is inferior to static gantry IMRT because the beam complexity metrics should not be used as a sole measure of plan quality. The increased beam complexity in VMAT is well compensated by reduced total number of beams and, thus, reduced treatment time. VMAT is an emergent technology, and we expect that its planning and delivery strategies will continue to improve. For example, a hybrid technique²⁰ that utilizes gantry angles continuously but differentially may achieve high delivery efficiency without increasing the complexity.

Beam complexity is generally thought to be related to the dose delivery accuracy. That is, complexity in IMRT beams compromises the accuracy of dose distributions that the patients actually receive. McNiven *et al.*¹⁸ reported no correlation between the IMRT gamma passing rates and the complexity metric MCS across multiple treatment sites. However, McGarry *et al.*¹⁹ suggested that lower IMRT gamma passing rate were associated with plans with higher beam complexity or lower MCS values. Younge *et al.*¹⁵ reported that plans with higher complexity or larger edge metric values led to greater percent of pixels with >10% dose errors. Our retrospective data showed that measured vs calculated dose differences were weakly correlated with PA, PM, and PMU. We attributed two major factors to this observation. First, our dose measurements had limitations. The ion chamber measurements were done at a single point per plan. This may underestimate the dose errors that occurred elsewhere, e.g., where the dose gradients were large. The film was used as a relative dose measurement. Normalization in film data processing may obscure the true dose errors.¹ In addition, a single percentage of pixels passing the gamma criterion may not be sensitive enough to detect the dose errors.^{21–23} Second, beam complexity is not the single source contributing to the dose errors. In fact, dose errors may arise from many measurement errors such as partial volume effect of ion chambers, film calibration uncertainty, MLC leaf position error, dose rate ramp up/down error, gantry sag or wobble, neglected couch attenuation, etc. Errors in TPS beam modeling and MLC modeling also contribute to the measured vs calculated dose discrepancies. Perhaps stronger correlation between beam

complexity and IMRT deliverability can be observed in a prospective study, in which the effect of beam complexity is isolated from many other sources of dose errors.

5. CONCLUSIONS

We have studied the complexity of IMRT beams by analyzing the averaged area, shape irregularity, and modulation of beam apertures. We found that the beam complexity was not equal among the prostate IMRT beams from different gantry angles. Among the three treatment sites studied, prostate IMRT plans had the smallest aperture irregularity, beam modulation, and normalized MU; HN IMRT plans had large beam irregularity and beam modulation; and spine stereotactic IMRT plans generally had small beam apertures, which may be associated with the relatively large discrepancies between planned and IMRT QA measured doses. Prostate VMAT beams showed larger shape irregularity and modulation than prostate step-and-shoot IMRT beams. Finally, we demonstrated that beam complexity was affected by the adjustments to planning parameters, including the minimum segment area, the number of optimization iterations, and the maximum number of segments. Quantification of beam complexity may be useful in guiding IMRT plan evaluation and ultimately reducing radiation dose uncertainties.

ACKNOWLEDGMENTS

The authors thank Zachary Bohannon and Kathryn Carnes for reviewing and scientific editing of this paper. The authors are grateful to the anonymous reviewers for their insightful comments and suggestions.

^{a)}Author to whom correspondence should be addressed. Electronic mail: wdu@mdanderson.org; Telephone: 713-745-7054.

¹G. A. Ezzell, J. W. Burmeister, N. Dogan, T. J. LoSasso, J. G. Mechalakos, D. Mihailidis, A. Molineu, J. R. Palta, C. R. Ramsey, B. J. Salter, J. Shi, P. Xia, N. J. Yue, and Y. Xiao, "IMRT commissioning: Multiple institution planning and dosimetry comparisons, a report from AAPM Task Group 119," *Med. Phys.* **36**, 5359–5373 (2009).

²J. M. Galvin, G. Ezzell, A. Eisbrauch, C. Yu, B. Butler, Y. Xiao, I. Rosen, J. Rosenman, M. Sharpe, L. Xing, P. Xia, T. Lomax, D. A. Low, and J. Palta, "Implementing IMRT in clinical practice: A joint document of the American Society for Therapeutic Radiology and Oncology and the American Association of Physicists in Medicine," *Int. J. Radiat. Oncol., Biol., Phys.* **58**, 1616–1634 (2004).

³M. Broderick, M. Leech, and M. Coffey, "Direct aperture optimization as a means of reducing the complexity of Intensity Modulated Radiation Therapy plans," *Radiat. Oncol.* **4**:8 (2009).

⁴C. X. Yu, D. A. Jaffray, and J. W. Wong, "The effects of intra-fraction organ motion on the delivery of dynamic intensity modulation," *Phys. Med. Biol.* **43**, 91–104 (1998).

⁵L. Court, M. Wagar, R. Berbeco, A. Reisner, B. Winey, D. Schofield, D. Ionascu, A. M. Allen, R. Popple, and T. Lingos, "Evaluation of the interplay effect when using RapidArc to treat targets moving in the craniocaudal or right-left direction," *Med. Phys.* **37**, 4–11 (2010).

⁶I. J. Das, C. W. Cheng, R. J. Watts, A. Ahnesjo, J. Gibbons, X. A. Li, J. Lowenstein, R. K. Mitra, W. E. Simon, and T. C. Zhu, "Accelerator beam data commissioning equipment and procedures: Report of the TG-106 of the Therapy Physics Committee of the AAPM," *Med. Phys.* **35**, 4186–4215 (2008).

⁷I. J. Das, G. X. Ding, and A. Ahnesjo, "Small fields: Nonequilibrium radiation dosimetry," *Med. Phys.* **35**, 206–215 (2008).

⁸O. A. Sauer and J. Wilbert, "Measurement of output factors for small photon beams," *Med. Phys.* **34**, 1983–1988 (2007).

⁹W. U. Laub and T. Wong, "The volume effect of detectors in the dosimetry of small fields used in IMRT," *Med. Phys.* **30**, 341–347 (2003).

¹⁰G. X. Ding, D. M. Duggan, and C. W. Coffey, "Commissioning stereotactic radiosurgery beams using both experimental and theoretical methods," *Phys. Med. Biol.* **51**, 2549–2566 (2006).

¹¹F. Sanchez-Doblado, R. Capote, A. Leal, J. V. Rosello, J. I. Lagares, R. Arrans, and G. H. Hartmann, "Microionization chamber for reference dosimetry in IMRT verification: Clinical implications on OAR dosimetric errors," *Phys. Med. Biol.* **50**, 959–970 (2005).

¹²G. S. Ibbott, D. S. Followill, H. A. Molineu, J. R. Lowenstein, P. E. Alvarez, and J. E. Roll, "Challenges in credentialing institutions and participants in advanced technology multi-institutional clinical trials," *Int. J. Radiat. Oncol., Biol., Phys.* **71**, S71–S75 (2008).

¹³M. Nauta, J. E. Villarreal-Barajas, and M. Tambasco, "Fractal analysis for assessing the level of modulation of IMRT fields," *Med. Phys.* **38**, 5385–5393 (2011).

¹⁴S. Pandya and J. Burmeister, "SU-GG-T-127: Effect of fluence smoothing on plan quality and delivery accuracy in intensity modulated radiotherapy," *Med. Phys.* **35**(6), 2755 (2008).

¹⁵K. C. Younge, M. M. Matuszak, J. M. Moran, D. L. McShan, B. A. Fraass, and D. A. Roberts, "Penalization of aperture complexity in inversely planned volumetric modulated arc therapy," *Med. Phys.* **39**, 7160–7170 (2012).

¹⁶S. Webb, "Use of a quantitative index of beam modulation to characterize dose conformity: Illustration by a comparison of full beamlet IMRT, few-segment IMRT (fsIMRT) and conformal unmodulated radiotherapy," *Phys. Med. Biol.* **48**, 2051–2062 (2003).

¹⁷M. M. Coselmon, J. M. Moran, J. D. Radawski, and B. A. Fraass, "Improving IMRT delivery efficiency using intensity limits during inverse planning," *Med. Phys.* **32**, 1234–1245 (2005).

¹⁸A. L. McNiven, M. B. Sharpe, and T. G. Purdie, "A new metric for assessing IMRT modulation complexity and plan deliverability," *Med. Phys.* **37**, 505–515 (2010).

¹⁹C. K. McGarry, C. D. Chinneck, M. M. O'Toole, J. M. O'Sullivan, K. M. Prise, and A. R. Hounsell, "Assessing software upgrades, plan properties and patient geometry using intensity modulated radiation therapy (IMRT) complexity metrics," *Med. Phys.* **38**, 2027–2034 (2011).

²⁰R. Li and L. Xing, "Bridging the gap between IMRT and VMAT: Dense angularly sampled and sparse intensity modulated radiation therapy," *Med. Phys.* **38**, 4912–4919 (2011).

²¹J. J. Kruse, "On the insensitivity of single field planar dosimetry to IMRT inaccuracies," *Med. Phys.* **37**, 2516–2524 (2010).

²²B. E. Nelms, H. Zhen, and W. A. Tome, "Per-beam, planar IMRT QA passing rates do not predict clinically relevant patient dose errors," *Med. Phys.* **38**, 1037–1044 (2011).

²³M. Stasi, S. Bresciani, A. Miranti, A. Maggio, V. Sapino, and P. Gabriele, "Pretreatment patient-specific IMRT quality assurance: A correlation study between gamma index and patient clinical dose volume histogram," *Med. Phys.* **39**, 7626–7634 (2012).